

Capillary breakup extensional rheometry (CaBER) on semi-dilute and concentrated polyethyleneoxide (PEO) solutions

Oliver Arnolds · Hans Buggisch ·
Dirk Sachsenheimer · Norbert Willenbacher

Received: 16 March 2010 / Revised: 14 September 2010 / Accepted: 16 October 2010 / Published online: 6 November 2010
© Springer-Verlag 2010

Abstract Semi-dilute ($c^* < c < c_e$) as well as concentrated, entangled ($c > c_e$) solutions of PEO yield uniformly thinning, cylindrical filaments in capillary breakup extensional rheometry (CaBER) experiments. Up to $c \approx c_e$ thinning can be characterized by a single elongational relaxation time λ_E . Comparison with the longest shear relaxation time, λ_S reveals that λ_E/λ_S decreases with increasing concentration or molecular weight according to $(c[\eta])^{-4/3}$. This is attributed to the large deformation the solutions experience during filament thinning. A factorable integral model including a single relaxation time and a Soskey or Wagner damping function accounting for the large deformation in CaBER experiments is used to calculate λ_E/λ_S and provides good agreement with experimental results. Irrespective of concentration or molecular weight a beads-on-a-string structure occurs prior to filament breakup at a diameter ratio $D/D_0 \approx 0.01$. This instability is supposed to be closely related to a flow-induced phase separation.

Keywords Elongational flow · Uniaxial extension · Relaxation time · Polymer solution

Introduction

Understanding elongational flow properties of polymer solutions is of great importance for many industrial applications such as ink jet printing, spraying, or coating. The earliest determinations of elongational viscosity were made for the simplest case of uniaxial extension. Trouton (1906) and many later investigators (James and Walters 1993) found that for incompressible Newtonian liquids, the elongational viscosity η_E is three times the shear viscosity η_S . Many materials including polymer melts and solutions exhibit shear-thinning in shear and strain-hardening in uniaxial extension. Even low to medium viscosity solutions may exhibit significant strain hardening effects if they include small amounts of high molecular weight polymer (Tirtaatmadja and Sridhar 1993; Solomon and Muller 1996).

Several devices for measuring the elongational viscosity of polymer solutions have been developed during the last decades. These techniques are often constrained by the difficulty of establishing and maintaining a uniform elongational flow field for long enough that a steady state can be reached (Bazilevsky et al. 1990; Stelter et al. 2000). The review of James and Walters (1993) surveys the difficulties inherent with devices such as opposed jet rheometers and contraction geometries. The experimental time and strain windows in the region of strong extension are limited and the path of a typical fluid element does not provide a motion with constant stretch history. Filament stretching devices have their genesis in the work of Matta and Tytus (1990) who suggested the use of a small cylindrical mass accelerating freely under gravity to stretch a small liquid bridge connecting the mass to a stationary support. Photographic analysis of the rate

O. Arnolds (✉) · H. Buggisch · D. Sachsenheimer · N. Willenbacher
Institute for Mechanical Process Engineering and Mechanics, Karlsruhe Institute of Technology, Gotthard-Franz-Str. 3, 76131 Karlsruhe, Germany
e-mail: Oliver.Arnolds@kit.edu

of decrease in filament radius was then used to compute an extensional stress growth under the action of a constant force. In the same year, Bazilevsky et al. (1990) described an extensional rheometer which is based on monitoring the diameter of a fluid drop initially confined between two parallel plates after a sudden separation of the plates. The thread is practically cylindrical in its centre and has a much smaller cross-sectional radius there than in the end regions attached to the plates. This filament shape results in a much higher capillary pressure in the thread than in the end regions and the fluid is squeezed toward the upper and lower plates. This creates an elongational flow which leads to self-thinning of the thread and the evolution of the thread diameter is observed while the thread thins and finally breaks. The easy handling, the small amount of sample needed for the experiment, the wide range of viscosities ($5 \cdot 10^{-2}$ – 10 Pa s) for which it is applicable, and the large Hencky strains, that are attainable (depending on fluid properties) are the most important advantages of this so-called capillary breakup extensional rheometry (CaBER). The technique has been applied to various kinds of complex fluids including carbon nanotube suspensions (Tiwari et al. 2009), concentrated emulsions (Niedziedz et al. 2009), crosslinked polymeric thickener solutions (Kheirandish et al. 2009), or wormlike micellar solutions (Yesilata et al. 2006; Rothstein 2009). But over the years, a strong focus was on weakly elastic fluids including aqueous solutions of poly(ethylene oxide) (PEO) (Bazilevskii

et al. 1997, Christanti and Walker 2001a, b; Rodd et al. 2005; Tirtaatmadja et al. 2006), poly(acrylamide) (PAAm), Xanthan (Stelter et al. 2000), polyelectrolyte complexes (Willenbacher et al. 2008) as well as acrylic thickeners (Kheirandish et al. 2008), and also solutions of poly(styrene) (PS) (Bazilevskii et al. 1997, Anna et al. 2001, Clasen et al. 2006a, b) and poly(isobutene) (PIB) (Liang and Mackley 1994) in organic solvents. These fluids form uniform, exponentially thinning cylindrical filaments; thus, the elongation rate $\dot{\epsilon}$ is constant throughout the filament and also in time. These fluids clearly exhibit strain hardening, but the calculation of an elongational viscosity is not straight forward, since the stress in axial direction T_{11} is not known. Nevertheless, a relaxation time λ_E characterizing the exponential decay of the filament diameter can be extracted. For a series of PIB solutions with different concentrations, Liang and Mackley (1994) found $\lambda_E \approx 3\bar{\lambda}_S$, with $\bar{\lambda}_S$ defined as an average relaxation time in shear. For PS Boger fluids with concentrations c around the critical overlap concentration c^* elongational relaxation times λ_E close to the longest Zimm relaxation time λ_Z were found by Bazilevskii et al. (1997), and for a PEO solution with $c \approx c^*$ Oliveira et al. (2006) report $\lambda_E \approx \lambda_S$, where λ_S is the longest relaxation time obtained from small amplitude oscillatory shear. On the other hand, it has been clearly shown for PEO (Tirtaatmadja et al. 2006, Christanti and Walker 2001a, b) as well as PS (Clasen et al. 2006a, b) solutions that the elongational relax-

Table 1 Physical properties of PEO solutions with $M_W = 10^6$ g/mol ($c^* = 0.41\%$, $c_e = 2.48\%$) and $M_W = 2 \cdot 10^6$ g/mol ($c^* = 0.24\%$, $c_e = 1.44\%$)

M_w /g/mol	$c/\%$	$c[\eta]/\text{ml/g}$	c/c^*	c/c_e	$\sigma/\text{mN/m}$	η_0/Pas	λ_S/ms	λ_E/ms	b/-	n/-
10^6	1.0	6.0	2.4	0.4	61.2	0.05 ± 0.01	11.4 ± 2.3	8.7 ± 1.3		
	1.5	9.0	3.7	0.6	61.3	0.15 ± 0.02	33.7 ± 6.7	12.4 ± 1.9	0.45	0.23
	2.0	12.0	4.9	0.8	62.2	0.40 ± 0.04	85 ± 17	16.4 ± 2.5	0.60	0.30
	2.5	15.0	6.1	1.0	63.7	1.00 ± 0.1	147 ± 29	24.7 ± 3.7	0.65	0.35
	3.0	17.9	7.3	1.2	53.7	2.61 ± 0.26	250 ± 50	49.3 ± 7.4		
	4.0	24	9.8	1.6	55.4					
	5.0	30	12.2	2.0	56.3					
+SDS	1.0	6.0	2.4	0.4	38.5	0.05 ± 0.01	12.2 ± 2.4	9.6 ± 1.4		
	2.0	12.0	4.9	0.8	38.2	0.39 ± 0.04	68 ± 14	16.3 ± 2.4		
$2 \cdot 10^6$	0.5	5.1	2.1	0.3	62.2	0.05 ± 0.01	19.4 ± 3.9	14.3 ± 2.1		
	1.0	10.3	4.2	0.7	65.7	0.22 ± 0.02	86 ± 17	32.8 ± 4.9		
	1.5	15.4	6.3	1.0	62.8	1.09 ± 0.10	431 ± 86	53.8 ± 8.1	0.54	0.27
	2.0	20.5	8.3	1.4	65.2	3.80 ± 0.40	1438 ± 287	150 ± 22	0.69	0.33
+SDS	1.0	10.3	4.2	0.7	38.5	0.20 ± 0.02	93 ± 19	25.6 ± 3.8		
	2.0	20.5	8.3	1.4	37.0	3.93 ± 0.40	1319 ± 264	138 ± 21		

The error in the surface tension is ± 1 mN/m, the error in η_0 , λ_E , and λ_S is calculated as the standard deviation from a set of at least three measurements. The power law exponents n and b for the damping functions according to Wagner and Soskey, respectively, as determined from steady shear viscosity data are also listed for those solutions for which the linear viscoelastic relaxation is well described by the Zimm model. The error for the parameters n and b is ± 0.02

ation time can vary significantly with concentration even far below c^* , and values $1 < \lambda_E/\lambda_Z < 10$ are reported for $0.01 < c/c^* < 1$, but also $\lambda_E/\lambda_Z < 1$ are documented for very dilute solutions down to concentrations of 0.2 ppm (Bazilevskii et al. 1997). So far, little is known about the relationship between shear and elongational relaxation time (as deduced from CaBER) for semi-dilute and concentrated solutions with $c \gg c^*$. For wormlike micellar surfactant solutions, $\lambda_E/\lambda_S \approx 1/3$ has been reported (Yesilata et al. 2006), which might be attributed to a breakup of micelles and structural changes in strong flows of these solutions. For aqueous solutions of acrylic polymeric thickeners known to form large intermolecular aggregates via hydrophobic interaction, very low ratios of $\lambda_E/\lambda_S < 0.1$ are found even for $c > c^*$ (Kheirandish et al. 2008). For solutions of poly(acrylic acid)-based polyelectrolyte complexes λ_E/λ_S ratios of around 1/4 have been observed (Willenbacher et al. 2008). But in both cases, the physical origin of these results remains unclear. It may be either due to flow-induced structural changes like breakup of aggregates/complexes or a limited extensibility of these objects due to internal attractive interactions not present in solutions of linear flexible polymers. Therefore, this paper focuses on the relationship between λ_E and λ_S for linear flexible polymers in the semi-dilute ($c^* < c < c_e$) and concentrated, entangled regime ($c > c_e$) and PEO/water is used as model system. We find that λ_E/λ_S strongly decreases with increasing concentration, and we discuss the relationship between λ_E and λ_S on the basis of a simple integral constitutive equation using a single relaxation time and a damping function h to account for the effect of the large deformations present in CaBER experiments. Finally, we report on the beads-on-a-string instability also occurring in these concentrated solutions prior to filament breakup. For viscoelastic fluids, this phenomenon has been described first by Goldin et al. (1969), and it has been studied intensively since then especially for dilute solutions of PEO (Christanti and Walker 2001a, b; Oliveira and McKinley 2005; Oliveira et al. 2006; Tirtaatmadja et al. 2006; Sattler et al. 2008), PS, or PAAm (Clasen et al. 2006a, b; Sattler et al. 2008) but also for wormlike micellar surfactant solutions (Sostarcez and Belmonte 2004). Classical stability analysis predicts less stability of viscoelastic compared to Newtonian fluids. But high stresses due to the elongation of polymer molecules (strain hardening) lead to a stabilization of filaments and the instability occurs, only when the extensibility limit of the molecules is reached. The formation of beads, the occurrence of satellite drops, and also so-called sub-main drops has been discussed intensively

within the framework of fluid mechanics (Christanti and Walker 2001a, b; Oliveira and McKinley 2005; Oliveira et al. 2006; Chang et al. 1999; Clasen et al. 2006a, b). Moreover, it has been directly shown that the beads-on-a-string structure can be accompanied by a flow-induced phase separation for $c > c^*$: the solvent is enriched in the beads, while the filaments connecting them mainly consist of highly extended polymer chains (Sattler et al. 2008). Here, we find that the droplet diameter is essentially independent of concentration and molecular weight of the dissolved polymer over a wide range of viscosities and relaxation times. These results support the earlier finding, that for semi-dilute and concentrated PEO solutions the phenomenon may be controlled by a demixing of polymer and solvent induced by the large elongational strain occurring during capillary thinning.

Materials and methods

Samples

PEO with average molecular weights of $2 \cdot 10^4$, 10^6 , $2 \cdot 10^6$, and $4 \cdot 10^6$ g/mol (Aldrich Chemical Co., UK) were supplied as powder and were used without further purification.

Aqueous solutions with different concentrations between 0.5 and 5 wt.% of PEO (depending on molecular weight) were prepared by dispersing the polymeric powder into distilled water and shaking at 350 rpm until the PEO was dissolved. The polymer concentrations were prepared as dry weight percentages and all the solutions were stored for at least 72 h at ca. 5°C before the rheological measurements were performed.

Solutions with reduced surface tension were prepared by adding 8 mmol/l of sodium dodecyl sulfate (SDS) to the solutions with 1% and 2% PEO concentration and $M_w = 10^6$ and $2 \cdot 10^6$ g/mol.

Surface tension

Surface tension Γ was determined experimentally using a DCAT 11 (DataPhysics) tensiometer with a platinum–iridium Wilhelmy-plate operating at room temperature. Surface tension is independent of molecular weight but decreases with increasing polymer concentration. Values between 53.7 and 65.7 mN/m have been measured for pure PEO solutions. Upon addition of SDS the surface tension was reduced to 37.0 mN/m. Data are summarized in Table 1. It is known that PEO and SDS can form complexes in aqueous solutions, which exhibit distinct rheological

properties (Miller and Cooper-White 2009). But this occurs at much higher SDS/PEO ratios, and no effect of SDS on flow properties has been observed for the PEO solutions investigated here.

Measurement techniques

Shear flow

Small amplitude oscillatory shear experiments were carried out using an ARES—rheometer (TA Instruments) equipped with cone-plate geometry (diameter $d = 50$ mm, cone angle $\alpha = 0.01$ rad) at $T = 20 \pm 0.2^\circ\text{C}$ using a water thermostat. Experiments were done in the linear response regime covering a frequency range from 0.01 to 100 rad/s. The instrument operates in a strain-controlled mode and amplitude sweeps at $\omega = 3.14$ rad/s were performed prior to each frequency sweep in order to identify the linear viscoelastic response regime. All frequency sweeps were done at strain amplitudes $\gamma_0 < 100\%$ to assure linear response.

Squeeze flow

Oscillatory squeeze flow experiments were performed using a piezo-driven axial vibrator (PAV) covering a frequency range from 100–36,000 rad/s. In these measurements, the sample is placed between two circular plates with a diameter of 20 mm and a gap of 31–58 μm , adjustable by different lids. The upper plate is screwed to the base plate. The lower plate is driven through two pairs of piezoelectric actuators. By applying a sinusoidal voltage via a lock-in amplifier, the plate oscillates about a mean position. Two further piezoelectric sensor pairs deliver the response signal. Empty cell measurements have to be performed as a reference in order to calculate the desired rheological properties from the ratio of the output voltage with and without sample U/U_0 and the corresponding phase shift $\varphi - \varphi_0$. Measurements were carried out at 20°C . Further information about the setup of the PAV device is available in Crassous et al. (2005).

Elongational flow

Characterization of elongational flow resistance was done with a CaBER-1 rheometer (Thermo Haake) equipped with plates of diameter $d = 6$ mm. Our instrument is equipped with a high-speed camera Fastcam-X 1024 PCI, a telecentric objective and blue telecentric background light. This setup allows to take up to 1,000 pictures per second with at a resolution of $1,024 \times$

1,024 pixel. Two objectives with fivefold and twentyfold magnification were used corresponding to an image resolution of 3.5 and 0.7 $\mu\text{m}/\text{pixel}$. The described setup allows for a simultaneous measurement of the filament diameter with the laser micrometer and video imaging at high reproducibility (Niedzwiedz et al. 2009).

The initial plate separation was chosen to be $h_0 = 3.0$ mm. A step strain was employed to create a liquid filament separating the plates from their initial distance h_0 to their final separation $h_f = 10.0$ mm within 40 ms at constant separating speed. This corresponds to a Hencky strain $m = 1.2$. In preliminary experiments, m was varied between 0.8 and 1.7 and the stretching time was varied between 20 and 60 ms, but no effect on the resulting relaxation time λ_E was found for the solutions investigated here.

Results and discussion

Relationship between shear and elongational relaxation time

For a Maxwell fluid, the decay of the diameter $D(t)$ of filament with initial diameter D_0 in a CaBER experiment can be described as McKinley and Tripathi (2000):

$$\frac{D(t)}{D_0} = 2 \left(\frac{GD_0}{4\Gamma} \right)^{\frac{1}{3}} \exp \left(-\frac{t}{3\lambda_E} \right) \quad (1)$$

Where λ_E is the elongational relaxation time governing the capillary breakup and G is the elastic modulus of the filament. The characteristic relaxation time λ_E is extracted from a fit of Eq. 1 to the experimental $D(t)$ data. Furthermore, λ_E is directly related to the elongation rate $\dot{\epsilon}$, which is constant throughout the filament and in time:

$$\dot{\epsilon}_0 = \frac{2}{3\lambda_E} = \text{const.} \quad (2)$$

For the normal stress, difference then holds:

$$\sigma \propto \exp \left(\frac{\dot{\epsilon}_0}{2} t \right) \quad (3)$$

In order to relate the elongational relaxation time λ_E to the characteristic shear relaxation time, we use a simple integral equation (Böhme 2000):

$$T = - \int_0^\infty \frac{dG}{ds} \left((1 - \psi) (C_t^{-1} - 1) h - \psi (C_t - 1) h \right) ds \quad (4)$$

Here, \mathbf{T} is the tensor of the extra stresses, ψ the ratio of the normal stress differences, \mathbf{C}_t the relative Cauchy–Green tensor, and h the damping function characterizing the nonlinear deformation behavior of the fluid. For uniaxial elongation, \mathbf{C}_t reads:

$$\mathbf{C}_t = \begin{pmatrix} \exp(-2\varepsilon) & 0 & 0 \\ 0 & \exp(\varepsilon) & 0 \\ 0 & 0 & \exp(\varepsilon) \end{pmatrix} \quad (5)$$

In the following, we assume that the normal stress difference $\psi = 0$ and that the linear viscoelastic shear modulus is characterized by a single relaxation time:

$$G = G_0 \exp\left(-\frac{s}{\lambda_S}\right) \quad (6)$$

with G_0 as elastic modulus and λ_S as shear relaxation time. According to Eq. 4, the normal stress difference in uniaxial elongation is then given by:

$$\sigma = T_{11} - T_{22} = - \int_0^\infty \frac{dG}{ds} (\exp(2\varepsilon) - \exp(-\varepsilon)) h \, ds \quad (7)$$

The initial step strain applied to the fluid prior to capillary thinning of the fluid filament in a CaBER experiment is expressed in terms of the delta-distribution $\delta(t)$:

$$\dot{\varepsilon} = \begin{cases} \varepsilon_i \delta(t) + \dot{\varepsilon}_0 & \text{for } t \geq 0 \\ 0 & \text{for } t < 0 \end{cases} \quad (8)$$

In this equation, ε_i characterizes the elongation in the initial step strain deformation. The total Hencky strain can be calculated as follows:

$$\varepsilon = \int_0^s \dot{\varepsilon}(t-s) ds = \begin{cases} \varepsilon_i & \text{for } s < t \\ \varepsilon_i + \dot{\varepsilon}_0 t & \text{for } s \geq t \end{cases} \quad (9)$$

Assuming a large ε_i and keeping in mind that the damping function can only depend on the invariants $I = \text{Tr } \mathbf{C}_t^{-1}$ and $II = \text{Tr } \mathbf{C}_t$, the integral Eq. 7 can be solved:

$$\sigma = G_0 h(I, II) \exp(2\varepsilon_i + 2\dot{\varepsilon}_0 t) \exp\left(-\frac{t}{\lambda_S}\right) \quad (10)$$

Soskey and Winter (1984) and Wagner and Demarmels (1990) have proposed two simple models relating the damping function h to the invariants of the Cauchy–Green tensor. The Soskey model reads:

$$h = \frac{1}{1 + a_s (J - 3)^b} \quad (11)$$

where a_s and b are material specific parameters characterizing the nonlinear flow behavior. In case of uniaxial elongation with:

$$I \approx \exp(2\varepsilon_i + 2\dot{\varepsilon}_0 t) \quad (12)$$

$$II \approx 2 \exp(\varepsilon_i + \dot{\varepsilon}_0 t) \quad (13)$$

$$J = (\alpha I + (1 - \alpha) II) \approx \alpha \exp(2\varepsilon_i + 2\dot{\varepsilon}_0 t) \quad (14)$$

we obtain for h :

$$h = \frac{1}{1 + a_s (\alpha J - 3)^b} \approx \frac{1}{a_s \alpha^b} \exp(-2\varepsilon_i b) \exp(-2\dot{\varepsilon}_0 b t) \quad (15)$$

Insertion into Eq. 10 provides the following relationship for the normal stress difference:

$$\sigma \propto \exp\left(2\dot{\varepsilon}_0(1 - b)t - \frac{t}{\lambda_S}\right) \quad (16)$$

Comparison of Eq. 16 with Eq. 3 yields:

$$\lambda_E = \lambda_S \left(1 - \frac{4}{3}b\right) \quad (17)$$

Note, for $h = 1$, our simplified analysis yields $\lambda_E = \lambda_S$.

The model parameters a_s and b can be determined from the steady shear viscosity $\eta(\dot{\gamma})$. The integral model defined by Eq. 4 combined with the Soskey damping function yields the following expression for $\eta(\dot{\gamma})$:

$$\eta = - \int_0^\infty \frac{dG}{ds} \frac{s}{1 + a(\dot{\gamma}s)^{2b}} ds \quad (18)$$

The Zimm model provides a good description of the linear viscoelastic shear modulus for solutions with $c \leq c_e$, and here, we have fitted the experimental $G''(\omega)$ data in order to determine the Zimm parameters needed to calculate $G(s)$ (Rubinstein and Colby 2003). Then, we have solved Eq. 18 by numerical integration using the Soskey parameters a_s and b as input, and these parameters have been varied until a minimum for the following expression was reached:

$$\sum_{i=1}^m \frac{|\eta_i - \bar{\eta}_i|}{\eta_i} = \min \quad (19)$$

Here, η_i is the measured viscosity at a certain shear rate, $\bar{\eta}_i$ the calculated viscosity for the pair of values a_s and

b at measuring point i , and m is the total number of measurement points.

The damping function proposed by Wagner and Demarmels (1990):

$$h = \frac{1}{1 + a_w ((I - 3)(II - 3))^n} \quad (20)$$

With the material-specific parameters, a_w and n yields the following relationship between λ_E and λ_S :

$$\lambda_E = \lambda_S(1 - 2n) \quad (21)$$

and the parameter n can be determined from $\eta(\dot{\gamma})$ as described above.

Shear rheometry

In Fig. 1, the zero shear viscosity for PEO solutions with $M_w = 2 \cdot 10^4$, 10^6 , and $2 \cdot 10^6$ g/mol is shown as a function of $c[\eta]$, using the relationship $[\eta] = 1.25 \cdot 10^{-4} M_w^{0.78}$ derived for PEO solutions in the range of $10^4 < M_w < 10^7$ g/mol (Bailey et al. 1958). The solutions investigated here cover a broad concentration range from the dilute regime ($c < c^*$) to semi-dilute conditions where molecules overlap but do not entangle ($c^* < c < c_e$) and the concentrated, entangled regime ($c > c_e$). The well-known scaling relations $\eta_0 \sim c^\alpha$ with $\alpha = 1, 2$, and $14/3$, for the different concentration ranges, are recovered, and our results are in good agreement with previous results (Rubinstein and Colby 2003). CaBER experiments will focus on the solutions of the PEO

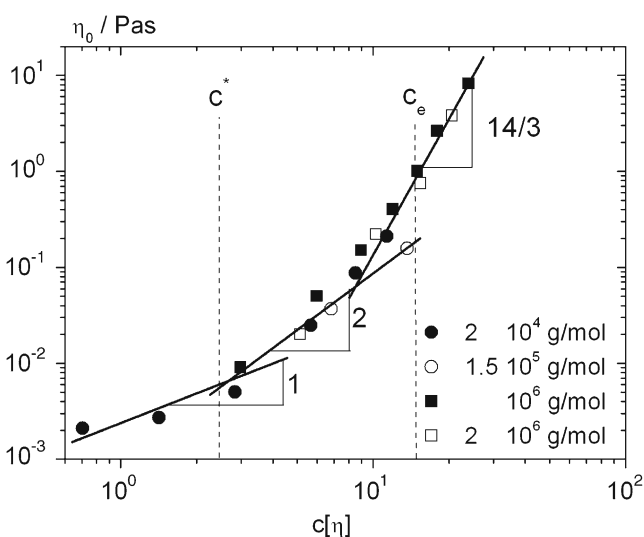


Fig. 1 Concentration dependence of zero shear viscosity of different PEO solutions with $M_w = 2 \cdot 10^4$ – $2 \cdot 10^6$ g/mol

grades with $M_w = 10^6$ g/mol with $[\eta] = 6.0$ ml/g and $2 \cdot 10^6$ g/mol with $[\eta] = 10.3$ ml/g and Fig. 1 demonstrates that all these solutions are well above c^* .

Figure 2 displays the absolute value of the complex viscosity $|\eta^*| = \omega^{-1} \sqrt{G'^2 + G''^2}$ as a function of angular frequency for a concentration series of PEO solutions with $M_w = 10^6$ g/mol, corresponding G' and G'' data are shown in Fig. 3. The solution with $c = 1\%$ shows the typical Zimm relaxation pattern with the scaling exponent $\nu = 0.59$ for a polymer in a good solvent, but for solutions with $c > 2\%$, a crossover of G' and G'' and the crossover frequency decreases with increasing concentration. This indicates that the polymer molecules start to entangle at $c \approx 2\%$. As expected pronounced shear thinning is observed for $c \geq c_e$. Similar results are obtained for solutions with $M_w = 2 \cdot 10^6$ g/mol. The characteristic shear relaxation time λ_S is calculated from the low frequency part of the data according to:

$$\lambda_S = \lim_{\omega \rightarrow 0} \frac{G'}{G''\omega} \quad (22)$$

This requires that the limiting scaling relations $G' \sim \omega^2$ and $G'' \sim \omega$ are valid. This is not the case for the highest concentrations for both molecular weights, and accordingly, no zero-shear plateau is reached in the examined frequency range in these cases. The characteristic longest relaxation time has been determined here for polymer concentrations up to 3% for $M_w = 10^6$ g/mol and up to 2% for $M_w = 2 \cdot 10^6$ g/mol. As expected, λ_S increases strongly with increasing polymer concentration

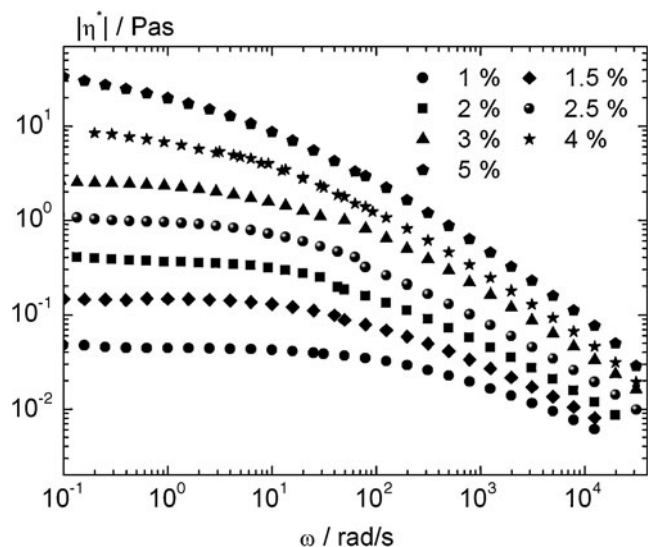


Fig. 2 Absolute value of complex viscosity $|\eta^*|$ vs. angular frequency ω for different PEO solutions with $M_w = 10^6$ g/mol

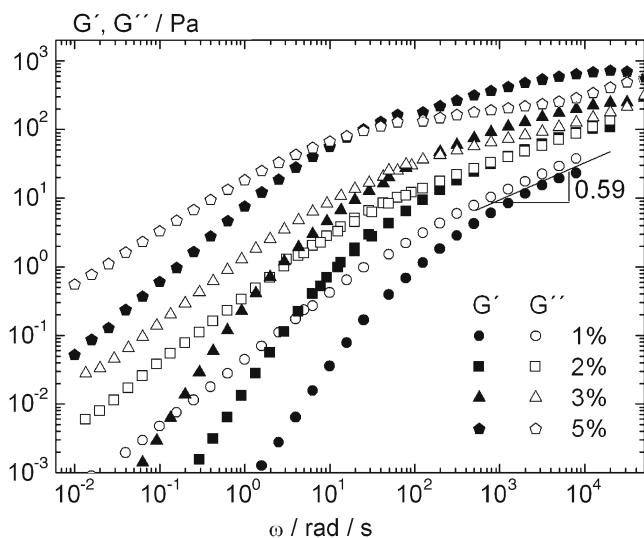


Fig. 3 Storage and loss modulus, G' and G'' vs. angular frequency ω for different PEO solutions with $M_w = 10^6$ g/mol

and molecular weight. This will be discussed in more detail below.

Elongational rheometry

All solutions investigated here form stable, liquid filament bridges in CaBER experiments, and after a short induction time, the filament shape is essentially cylindrical except for the regions close to the endplates. The initial filament midpoint diameter D_0 is mainly controlled by the ratio h_f/h_0 and lies in the range of $D_0 \approx 1.0\text{--}1.2$ mm. The time evolution of the normalized filament diameter $D(t)/D_0$ for solutions with $M_w = 10^6$ g/mol are shown Fig. 4. Obviously, filament lifetime strongly increases with increasing polymer concentration. But the filaments break at an essentially constant ratio $D/D_0 \approx 5 \cdot 10^{-3}$. This is in contrast to the behavior e.g. of the thickener solutions investigated before (Kheirandish et al. 2008). For these solutions, a strong increase of the maximum attainable Hencky strain with increasing polymer concentration was observed. We attribute this difference to the fact that filament breakup of the PEO solutions is preceded by the occurrence of a bead-on-a-string instability, which will be discussed

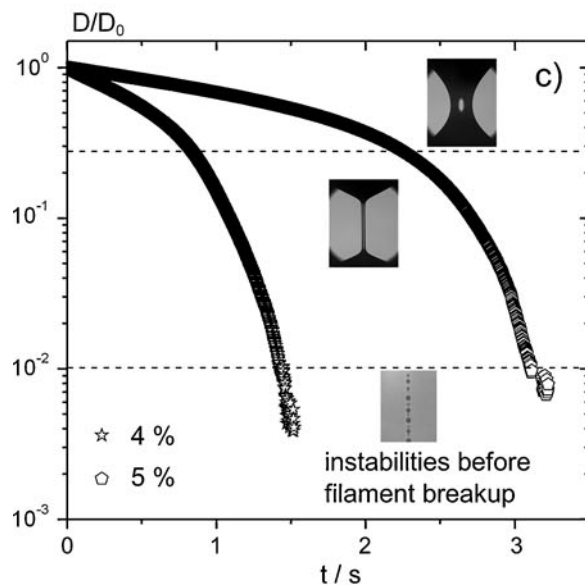
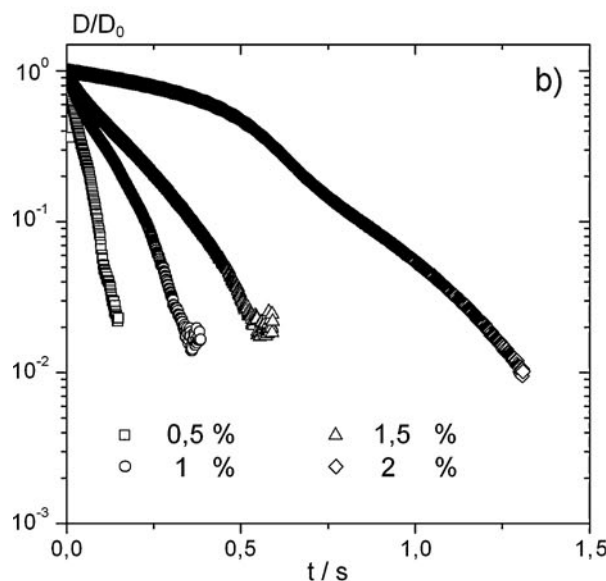
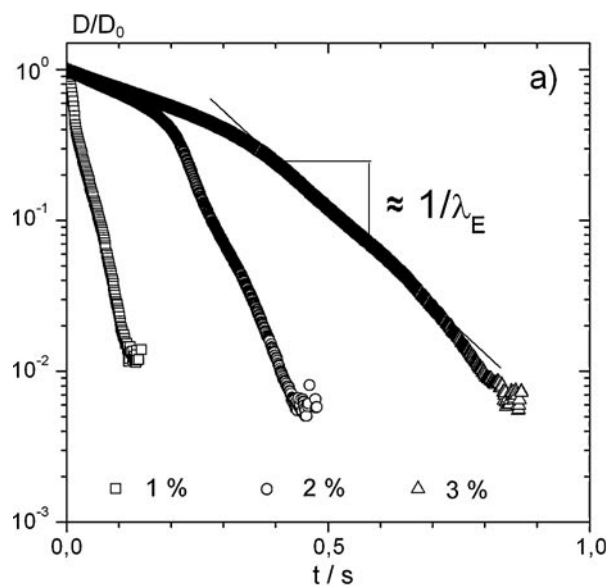


Fig. 4 Normalized filament diameter in CaBER experiments for PEO solutions. The time $t = 0$ is defined as the time at which the upper plate has reached its final position. **a** $M_w = 10^6$ g/mol and $c = 1\%$, 2% , 3% ; **b** $M_w = 2 \cdot 10^6$ g/mol and $c = 0.5\text{--}2\%$; **c** $M_w = 10^6$ g/mol and $c = 4\%$, 5% . Images of the characteristic filament shape at different stages of thinning are shown as insert in **c**, the different regimes of filament thinning are separated by dashed lines

in more detail below, whereas the thickener solutions mentioned above did exhibit homogeneous thinning throughout the whole diameter range down to 10 μm . For concentrations $c \leq 3\%$, an intermediate regime occurs between the initial induction period and the onset of the instability, in which filament thinning can be described by a single exponential. In this regime, the characteristic elongational relaxation time λ_E is determined according to Eq. 1. For concentrations $c > 3\%$, the filaments still exhibit a cylindrical shape in this intermediate regime, but there is no distinct period showing exponential filament thinning, and it is meaningless to extract a single characteristic relaxation time in these cases. Similar results are obtained for the solutions with $M_W = 2 \cdot 10^6$ g/mol; in this case, exponential thinning is observed up to $c = 2\%$ and a more complex filament decay for $c > 2\%$. This corresponds to the results from oscillatory shear, where λ_S could be determined only up to 3% and 2%, respectively, depending on molecular weight of the polymer. A comparison of characteristic relaxation times in shear and elongational flow is shown in Fig. 5 for the concentration row of PEO solutions with $M_W = 10^6$ g/mol. Characteristic scaling laws $\lambda_S \sim c^{(8/3 \pm 1/3)}$ and $\lambda_E \sim c^{(4/3 \pm 1/3)}$ are found. The scaling exponent for λ_S is in good agreement classical theory of polymer dynamics (Rubinstein and Colby 2003). Remarkably, we always observe higher relaxation times in oscillatory shear than in elongational measurements for the solutions investigated here, and the ratio λ_E/λ_S decreases with increasing concentration or molecular weight according a power law $\lambda_E/\lambda_S \sim c^{-4/3}$ as shown in Fig. 6. At concentrations close to c^* the ratio λ_E/λ_S

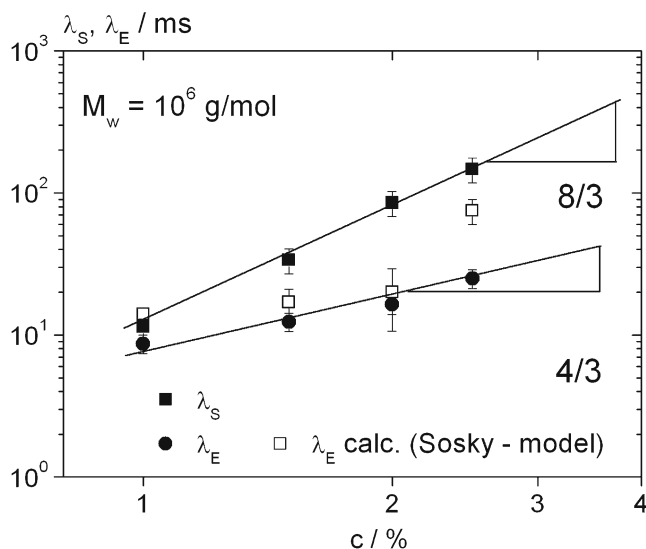


Fig. 5 λ_E and λ_S vs. concentration for $M_W = 10^6$ g/mol

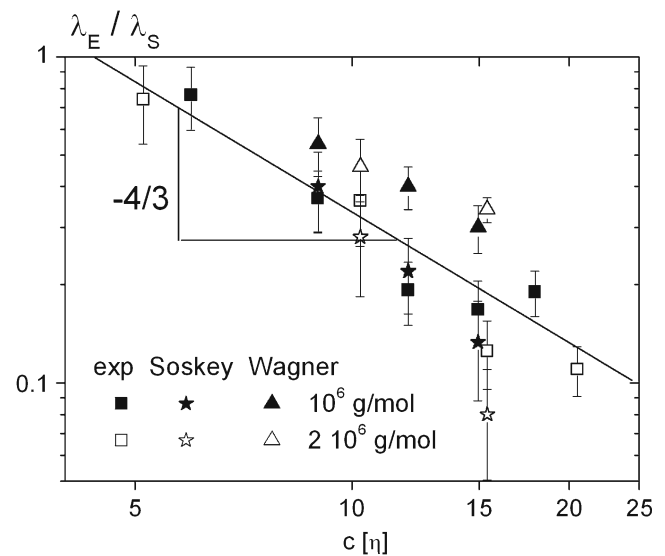


Fig. 6 Ratio λ_E/λ_S vs. concentration times intrinsic viscosity for solutions with $M_w = 10^6$ g/mol (open symbols) and $2 \cdot 10^6$ g/mol (closed symbols). Experimentally determined values (squares) are compared to those calculated based on the Soskey model (Eq. 17, stars) and the Wagner model (Eq. 21, triangles) with λ_S taken from the experiments

is close to one in accordance with earlier findings for polystyrene Boger fluids (Anna et al. 2001) and aqueous PEO solutions (Oliveira et al. 2006) with $c \approx c^*$. The strong decay of λ_E/λ_S with $c[\eta]$ might presumably be due to the strong non-linear behavior at large deformations occurring for solutions with $c \gg c^*$, but not in the dilute case. We have tried to estimate these effects employing a simple integral constitutive equation including a damping function h , which accounts for the nonlinear fluid response. In the limit of large deformations, this results in the linear relationship between λ_E and λ_S given in Eqs. 17 and 21 for the Soskey and Wagner model, respectively. The parameters b and n are extracted from the viscosity versus shear rate data as described in “Relationship between shear and elongational relaxation time” (Eqs. 18 and 19) for the solutions with concentrations $c < c_e$. Only in these cases where filament thinning can be characterized by a single relaxation time λ_E , the analysis of the λ_E/λ_S ratio makes sense. For these solutions $G(s)$ is well represented by the Zimm model. We take advantage of the Cox–Merz rule and determine b and n from the $|\eta^*|$ vs. ω curves shown in Fig. 2. Since the relevance of nonlinearities increases with c , the calculated ratio λ_E/λ_S decreases with increasing c . Figure 6 compares the λ_E/λ_S values directly obtained from shear and elongational measurements with those calculated using the Soskey Eq. 17 and Wagner Eq. 21 damping functions

with λ_S taken from the experiments. Obviously, the simple considerations based on a factorable integral constitutive equation including a damping function capture the right trend of a λ_E/λ_S ratio decreasing with increasing concentration. The predictions based on the Soskey model agree very well with the experimental data, whereas the λ_E/λ_S ratios calculated using the Wagner model are slightly higher than the experimental data. The phenomenological origin of both models prohibits further interpretation of these differences. Similarly low λ_E/λ_S ratios have been reported previously for aqueous solutions of high molecular weight poly(acrylic acid) as well as polyelectrolyte complexes based on it (Willenbacher et al. 2008). The low λ_E values found in these solutions of linear flexible polymers seem to be due to the strong nonlinear deformation the fluids experience in CaBER experiments. Much lower λ_E/λ_S ratios have been found for commercial acrylic thickener solutions (Kheirandish et al. 2008). These polyelectrolytes are known to form large aggregates due to hydrophobic interactions and in the cases the low λ_E/λ_S ratios may be due to structural changes induced by the strong elongational deformation during capillary thinning. Understanding the physical meaning of λ_E is crucial for the interpretation of CaBER experiments and obviously requires careful experimental as well as theoretical investigations.

For all solutions investigated here, irrespective of concentration or molecular weight, filament breakup is induced by the occurrence of an instability, which results in a beads-on-a-string structure as shown in Fig. 4c. For viscoelastic fluids, this phenomenon has been described first by Goldin et al. (1969), and it has been studied intensively since then (e.g., Chang et al. 1999; Christanti and Walker 2001a, b; Oliveira and McKinley 2005; Oliveira et al. 2006; Clasen et al. 2006a, b; Sattler et al. 2008). For PEO solutions with $c < c^*$, the formation of beads has been investigated intensively (Christanti and Walker 2001a, b; Oliveira and McKinley 2005; Oliveira et al. 2006). For PEO solutions with $c \approx c^*$, it has been directly shown, that the beads-on-a-string structure is accompanied by a flow-induced phase separation: the solvent is enriched in the beads, while the filaments connecting them mainly consist of highly extended polymer chains (Sattler et al. 2008). Here, we find, that the beads-on-a-string instability is pertinent even at concentrations $c \gg c^*$. In Fig. 7, the diameter of the main beads is displayed as a function of $c[\eta]$ and an image of the beads-on-a-string structure for a solution with $c = 2\%$ and $M_w = 2 \cdot 10^6$ g/mol is shown as insert. Obviously, D_{droplet} varies only in a narrow range between 5 and 10 μm . It seems to increase only weakly with increasing $c[\eta]$; hence, the onset of

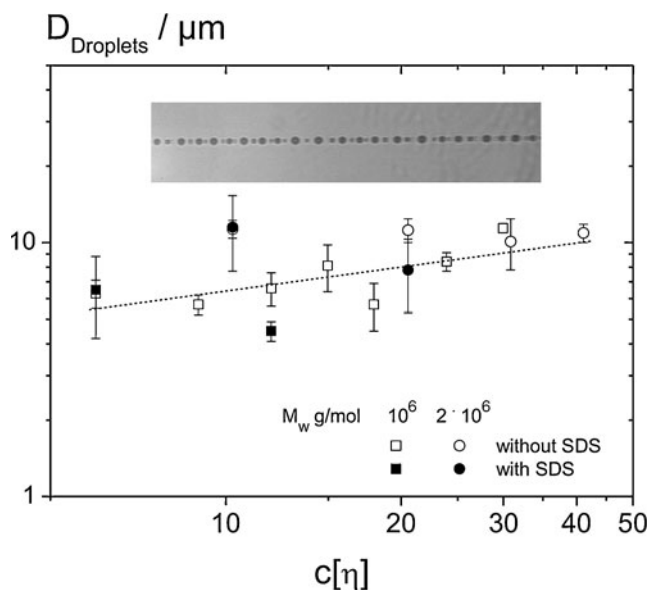


Fig. 7 Droplet sizes after filament breakup for PEO solutions with $M_w = 10^6$ g/mol and $M_w = 2 \cdot 10^6$ g/mol. Line is to guide the eye

the instability occurs at slightly higher diameter values as $c[\eta]$ increases. This is remarkable, since the solution viscosity and correspondingly the Ohnesorge number $Oh = \eta/(\rho\Gamma D)^{1/2}$, which is usually used to characterize breakup of filaments or jets, varies by about three orders of magnitude in the investigated $c[\eta]$ range. Also, the Deborah number $De = \lambda_S \cdot \dot{\epsilon}$ relevant for filament breakup in viscoelastic liquids increases from about 1 to 10 as $c[\eta]$ increases. Finally, also the surface tension (varied here by a factor of 3/5 due to the addition of SDS) and accordingly the capillary number $Ca = \eta\dot{\epsilon}D/\Gamma$ seem to have no significant effect on the occurrence of the beads-on-a-string instability. These results support the earlier result, that for solutions with $c > c^*$ the phenomenon could be controlled by flow-induced phase separation, which is mainly determined by the total strain the filament experiences. Phase separation is even more likely at the high polymer concentrations investigated here, than at the concentrations $c \approx c^*$ investigated by Sattler et al. (2008). At this point, we also note that the filament breakup observed in CaBER experiments on acrylic thickener solutions (Kheirandish et al. 2008) is different in nature. Despite their intermolecular aggregation and high apparent molecular weight, these thickener solutions are not entangled. They thin homogeneously and break at a critical $D(t)/D_0$ ratio which decreases with increasing polymer concentration, but at all investigated concentrations, this critical $D(t)/D_0$ ratio is clearly higher than the value found for the PEO solutions investigated here and no beads-on-a-string instability is observed.

Conclusion

We have characterized the elongational flow behavior of semi-dilute and concentrated, entangled solutions of high molecular weight PEO using the CaBER technique. We have covered the concentration range $0.7 < c[\eta] < 30$ and all investigated solutions form uniform cylindrical filaments which self-thin down to a diameter of about 5–10 μm . Then a beads-on-a-string structure occurs prior to filament breakup. Up to concentrations $c \approx c_e$, the filament diameter decays exponentially and is characterized by a single characteristic relaxation time λ_E . Comparing these λ_E data to the longest characteristic relaxation time λ_S from small amplitude oscillatory shear reveals that $\lambda_S \sim c^{8/3}$, whereas $\lambda_E \sim c^{4/3}$. For $c \approx c^*$, the ratio λ_E/λ_S is close to one in agreement with earlier results (Oliveira et al. 2006), but then strongly decreases according to $(\lambda_E/\lambda_S) \sim c^{-4/3}$. We have used a simple factorable integral constitutive equation in order to establish a relationship between λ_E and λ_S . This model includes a single relaxation time characterizing the linear response and a damping function h to account for the large strains occurring in CaBER experiments. The Soskey and Wagner model, respectively, have been employed to quantify h and the corresponding model parameters have been deduced from the shear viscosity. This both models provide ratios $\lambda_E/\lambda_S < 1$ that agree well with those found experimentally for $c \leq c_e$, agreement with experimental data is slightly better for the Soskey model than for the Wagner model. The size of the beads occurring prior to filament breakup is essentially independent of polymer concentration or molecular weight, values between 5 and 10 μm are found. This is remarkable since our solution series covers a broad range of viscosities and relaxation times, and obviously classical dimensionless numbers like the Ohnesorge or Deborah number used to characterize filament or jet breakup phenomena are not relevant here. This supports the earlier result for solutions with $c \approx c^*$ (Sattler et al. 2008) that the beads-on-a-string structure could be due to a flow-induced phase separation.

Acknowledgements We thank F. Bossler for his help in sample preparation and performing shear and CaBER experiments. S. Pfeiffer and C. Woodson are thanked for programming the analysis software. We appreciate valuable discussions with Prof. M. Wagner, Dr. K. Niedzwiedz and Dr. B. Hochstein. Prof. Wagner drew our attention to the appropriate determination of the damping function parameters from the shear viscosity function.

References

- Anna SL, McKinley GH et al (2001) Elasto-capillary thinning and breakup of model elastic liquids. *J Rheol* 45:115–138
- Bailey FE, Kucera JL, Imhof LG (1958) Molecular weight relations of poly(ethylene) oxide. *J Polym Sci* 32:517–518
- Bazilevsky AV, Entov VM, Rozhkov AN (1990) Liquid filament microrheometer and some of its applications. In: Oliver DR (ed) Third European rheology conference. Elsevier, San Diego, pp 41–43
- Bazilevskii AV, Entov VM et al (1997) Failure of polymer solution filaments. *Polym Sci A* 39:316–324
- Böhme G (2000) *Strömungsmechanik nichtnewtonischer Fluide*. Teuber, Stuttgart
- Chang HC, Demekhin EA, Kalaidin E (1999) Iterated stretching of viscoelastic jets. *Phys Fluids* 11:1717
- Christanti Y, Walker LM (2001a) Surface tension driven jet break up on strain-hardening solutions. *J Non-Newton Fluid Mech* 100:9–26
- Christanti Y, Walker LM (2001b) Effect of fluid relaxation time of dilute polymer solutions on jet breakup due to a forced disturbance. *J Rheol* 46:733–748
- Clasen C, Eggers J, Fontelos MA, Li J, McKinley GH (2006a) The beads on-string structure of viscoelastic threads. *J Fluid Mech* 556:283–308
- Clasen C, Plog JP et al (2006b) How dilute are dilute solutions in extensional flows? *J Rheol* 50:849–881
- Crassous JJ, Régisser R, Ballauff M, Willenbacher N (2005) Characterization of the viscoelastic behaviour of complex fluids using the piezoelectric axial vibrator. *J Rheol* 49:851–863
- Goldin M, Yerushalmi J, Pfeffer R, Shinnar R (1969) Breakup of laminar capillary jet of a viscoelastic fluid. *J Fluid Mech* 38:689–711
- James DF, Walters K (1993) A critical appraisal of available methods for the measurement of extensional properties of mobile systems. *Techniques in Rheological Measurements*. Elsevier, London, pp 33–53
- Kheirandish S, Gubaydullin I, Willenbacher N (2008) Shear and elongational flow behaviour of acrylic thickener solutions, Part I: effect of intermolecular aggregation. *Rheol Acta* 49:397–407
- Kheirandish S, Gubaydullin I et al (2009) Shear and elongational flow behavior of acrylic thickener solutions, Part II: effect of gel content. *Rheol Acta* 48:397–407
- Liang RF, Mackley MR (1994) Rheological characterization of the time and strain dependence for polyisobutylene solutions. *J Non-Newton Fluid Mech* 52:387–405
- Matta J, Tytus RP (1990) Liquid stretching using a falling cylinder. *Non-Newtonian Fluid Mech* 35:215–229
- McKinley G, Tripathi A (2000) How to extract the Newtonian viscosity from capillary breakup measurements in a filament rheometer. *J Rheol* 44(3):653–670
- Miller E, Cooper-White J (2009) The effects of chain conformation in the microfluidic entry flow of polymer-surfactant systems. *Non-Newtonian Fluid Mech* 160:22–30
- Niedzwiedz K, Arnolds O, Willenbacher N, Brummer R (2009) How to characterize yield stress fluids with Capillary Breakup Extensional Rheometry (CaBER)? *Appl Rheol* 19:41969–1–41969–10
- Oliveira MSN, McKinley GH (2005) Iterated stretching and multiple beads-on-string phenomena in dilute solutions of highly extensible flexible polymers. *Phys Fluids* 17:071704

- Oliveira MSN, Yeh R, McKinley GH (2006) Iterated stretching, extensional rheology and formation of beads-on-string structures in polymer solutions. *J Non-Newton Fluid Mech* 137:137–148
- Rodd LE, Scott JJ et al (2005) Capillary break-up rheometry of low-viscosity elastic fluids. *Appl Rheol* 15:12–27
- Rothstein JP (2009) Strong flows of viscoelastic wormlike micelle solutions. In: Binding DM, Walters K (eds) *Rheology review*. The British Society of Rheology, Aberystwyth, pp 1–42
- Rubinstein M, Colby RH (2003) *Polymer physics*. Oxford University Press, Oxford
- Sattler R, Wagner C, Eggers J (2008) Blistering pattern and formation of nanofibers in capillary thinning of polymer solutions. *Phys Rev Lett* 100:164502
- Solomon MJ, Muller SJ (1996) The transient extensional behaviour of polystyrene-based Boger fluids of varying solvent quality and molecular weight. *J Rheol* 40(5):837–856
- Soskey PR, Winter HH (1984) Large step shear strain experiments with parallel-disk rotational rheometers. *J Rheol* 29:625–645
- Sostarcez MC, Belmonte A (2004) Beads-on-string phenomena in wormlike micellar fluids. *Phys Fluids* 16:67
- Stelter M, Brenn G, Yarin AL, Singh RP, Durst F (2000) Validation and application of a novel elongational device for polymer solutions. *J Rheol* 44:595–616
- Tirtaatmadja V, Sridhar T (1993) A filament stretching device for measurement of extensional viscosity. *J Rheol* 37:1081–1102
- Tirtaatmadja V, McKinley GH, Cooper-White JJ (2006) Drop formation and breakup of low viscosity elastic fluids: effects of molecular weight and concentration. *Phys Fluids* 18:043101
- Tiwari MK, Bazilevsky AV, Yarin AL, Megaridis CM (2009) Elongational and shear Rheology of carbon nanotube suspensions. *Rheol Acta* 48:597–609
- Trouton FT (1906) On the coefficient of viscous and its relation to that of viscosity. *Proc R Soc Lond, A* 77(Iss 519):426–440
- Wagner MH, Demarmels A (1990) A constitutive analysis of extensional flows of polyisobutylene. *J Rheol* 34:943–958
- Willenbacher N, Matter Y, Gubaydullin I (2008) Effect of aggregation on shear and elongational flow properties of acrylic thickeners. *K-A Rheol J* 20:109–116
- Yesilata B, Clasen C, McKinley GH (2006) Nonlinear shear and extensional flow dynamics of wormlike surfactant solutions. *J Non-Newton Fluid Mech* 133:73–90